Influence of mixing and solid concentration on sodium bicarbonate secondary nucleation rate in stirred tank: theoretical and experimental studies

C. Wylock[*,1], V. Gutierrez[2], F. Debaste[1], T. Cartage[3], M.-P. Delplancke-Ogletree[2] and B. Haut[1]

[1] Transfers, Interfaces and Processes – Chemical Engineering Unit, ULB, 50 av. F.D. Roosevelt, CP 165/67, 1050 Brussels, Belgium
[2] Chemicals and Materials Department, ULB, 50 av. F.D. Roosevelt, CP 165/63, 1050 Brussels, Belgium
[3] Solvay SA, rue de Ransbeek 310, 1120 Brussels, Belgium

Received zzz, revised zzz, accepted zzz
Published online zzz

Key words Sodium bicarbonate, stirred tank crystallizer, secondary nucleation rate, computer simulation.

This work aims to investigate the influence of the solid concentration in suspension on the contact secondary nucleation rate of sodium bicarbonate crystallization in a stirred tank crystallizer and to show the necessity of a local description of the mixing for a nucleation rate influence study. Experiments and computational fluid dynamics (CFD) simulations are realized. Crystallization kinetic parameters are extracted from experimental data using a mass distribution fitting approach. CFD and the experimental results allow identifying that a mixing property correlated with the measurements of the secondary nucleation rate in the stirred tank crystallizer appears to be the turbulent dissipation rate on the edge of the impeller. Its influence and the influence of the solid concentration in the suspension on the secondary nucleation rate are estimated by the evaluation of their exponents in a kinetic law. The obtained exponent values are then discussed qualitatively.

1 Introduction

1.1 Framework: the refined sodium bicarbonate production process

The sodium bicarbonate ($NaHCO_3$) production process is one of the oldest processes of the Solvay group (more than one century). Sodium bicarbonate has numerous applications. It is used as an environmentally-friendly product for cleaning a wide range of surfaces or for neutralisation of acids in exhaust flue gas of numerous industries. It is also used in many everyday applications (cleaning agent, toiletry, food additive...).

The main step of the refined sodium bicarbonate production process is the dispersion of a gaseous mixture of nitrogen (N_2) and carbon dioxide (CO_2) in an aqueous solution of sodium carbonate (Na_2CO_3) and $NaHCO_3$. This dispersion is realized in large bubble columns (20 meter high and 2 meter large), called the BIR columns. A gas-liquid mass transfer of CO_2 occurs in the column. In the liquid phase, the following global reaction is taking place:

$$Na_2CO_3 + CO_2 + H_2O \rightarrow 2\ NaHCO_3 \qquad (1)$$

This reaction creates a supersaturation of $NaHCO_3$ in the liquid, resulting in the continuous precipitation of solid $NaHCO_3$, by a contact secondary nucleation process [1].

Since new applications of $NaHCO_3$ require high purity level and a well-defined crystal size distribution (CSD), Solvay is seeking a better understanding of the $NaHCO_3$ crystallization and is expecting the

[*] Corresponding author: e-mail cwylock@ulb.ac.be, Phone: +32 2 650 40 96, Fax: +32 2 650 29 10

This is the preprint version of a manuscript published in Crystal Research and Technology 45 (2010), no 9, p. 929-938
DOI: 10.1002/crat.201000233
Link: http://onlinelibrary.wiley.com/doi/10.1002/crat.201000233/abstract

development of a mathematical model of the BIR columns that could be used to optimize the process and to control the CSD from the operational conditions.

This model is the final goal of collaboration between the Solvay group and the Université Libre de Bruxelles. The expected gains using this model are a technological optimization, cost and time saving and, in a close future, new and improved products.

1.2 Objectives of the work

A previous work has shown that the crystallization kinetics of $NaHCO_3$ depends on several parameters, such as the temperature, the supersaturation, the solid concentration and the mixing [1]. The development of a $NaHCO_3$ crystallization kinetic model requires an accurate quantification of the influence of each parameter. In the BIR columns, the slowest stage of the process is the gas-liquid CO_2 absorption [2]. Therefore, the crystallization is limited by the gas-liquid CO_2 absorption.

As the CO_2 absorption rate is rather slow, it is difficult to control the supersaturation level in a lab-scale gas-liquid-solid reactor and consequently to study the supersaturation influence on the crystallization kinetics. Therefore, the $NaHCO_3$ crystallization is studied in a stirred tank crystallizer. This crystallizer is scaled to reproduce the same levels of supersaturation, of solid concentration and of volumetric dissipated power than in the BIR columns [1].

The objective of this paper is, on one hand, to understand and to quantify the influence of the solid concentration in the suspension on the contact secondary nucleation rate of $NaHCO_3$ in the stirred tank crystallizer and, on the other hand, to underline the necessity of local description of the mixing in the crystallizer for the nucleation rate study. This is the first step towards the understanding of the secondary nucleation rate of sodium bicarbonate in the BIR columns.

The study of the mixing in the stirred tank is not directly relevant for industry but it is necessary to allow an accurate quantification of the influences of the temperature, the supersaturation and the solid concentration on the growth rate and the nucleation rate of $NaHCO_3$, which will be investigated in a future work. Moreover, this mixing study provides a contribution to the fundamental understanding of the flow influence on the secondary nucleation rate in a stirred tank crystallizer.

Three work packages are performed. First, experiments are realized in the stirred tank reactor, for different solid concentration in suspension and for different flow conditions. The second package is the crystallization kinetic parameter extraction from the experimental results. A mass distribution fitting method is used to extract nucleation rates from crystal mass measurements on sieves. The last work package is the characterization of the global and the local flow properties in the tank. Indeed, it has been shown in the last decades that the secondary nucleation rate can depend on local flow properties [3-5]. Therefore, CFD simulations of the stirred tank crystallizer are performed with the FLUENT 6.3 software.

The combination of the three work packages allows identifying the relevant flow parameter and discussing qualitatively the solid concentration and the mixing influences from the obtained values.

2 Material and measurements

2.1 Raw materials

All the solutions are prepared with high purity water and high quality (pharmaceutical grade) $NaHCO_3$ (BICAR® SOLVAY, $NaHCO_3$ > 99.5%).

2.2 Experimental setup

A double jacket 5 dm^3 stirred tank crystallizer, with 4 dm^3 of active volume, was used for all the experiments. This crystallizer is isothermal and equipped with a draft tube located centrally in the vessel and four vertical baffles. The temperature of the solution in the crystallizer was 45°C. In order to increase the mixing capacity, a W form bottom was used [6]. The mixing was performed by a 3-blade marine propeller. It is covered with a Halar layer to limit the nucleation on its surface. A block-diagram of the experimental set-up is presented in Fig. 1.

This is the preprint version of a manuscript published in Crystal Research and Technology 45 (2010), no 9, p. 929-938
DOI: 10.1002/crat.201000233
Link: http://onlinelibrary.wiley.com/doi/10.1002/crat.201000233/abstract

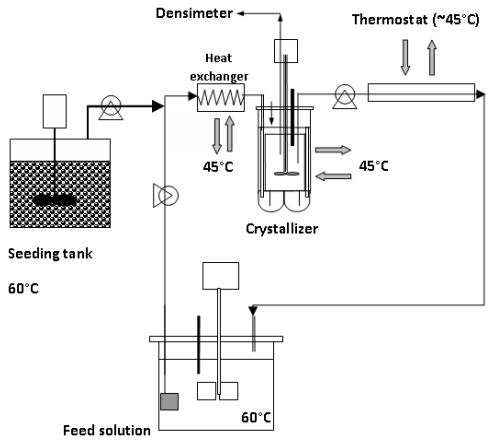

Fig. 1 Block diagram of the experimental set-up.

The experiments were operated in a continuous mode: the solution flow rate was equals to the suspension withdrawal flow rate. Therefore, the volume of the suspension in the crystallizer could be considered as being time independent.

The solution leaving the feed solution tank (see Fig. 1), called the feed solution, was saturated in $NaHCO_3$, at 60 °C, its Na_2CO_3 concentration was close to 10 g per kg of solution and it contained no solid phase.

After leaving the feed solution tank (at a flow rate Q_{feed}), this feed solution flowed through a heat-exchanger (see Fig. 1) where it was cooled to a temperature of 45°C (the crystallizer is also thermostated at 45°C) before being introduced in the crystallizer. A decrease in temperature of 15°C leads to a supersaturation of approximately 0.18 at the crystallizer entrance. After an induction period, crystals appear in the crystallizer through a mechanism of primary nucleation, quickly supplanted by secondary nucleation as the solid concentration in the crystallizer increases and as the supersaturation in the crystallizer decreases.

The propeller minimum rotation speed to avoid sedimentation was estimated by the procedure proposed by Mersmann et al. [7]. The estimated value was close to 200 rpm. However, it was observed that the suspension was not homogeneous using this rotation speed. This last was then increased until a homogeneous suspension was observed, with a safety margin [8]. Therefore, in this study, the propeller rotation speed is set equal or superior to 600 rpm.

When steady state was reached, after approximately 4 h, the $NaHCO_3$ concentration in the crystalliser was measured by titration and the supersaturation S was estimated using the following equation:

$$S \approx \frac{\left[\mathrm{NaHCO_3}\right] - \left[\mathrm{NaHCO_3}\right]_{sat}}{\left[\mathrm{NaHCO_3}\right]_{sat}} \tag{2}$$

where $[NaHCO_3]$ is the $NaHCO_3$ concentration in the liquid in the crystallizer and $[NaHCO_3]_{sat}$ is the $NaHCO_3$ saturation concentration for the considered Na_2CO_3 concentration and the considered temperature. $[NaHCO_3]_{sat}$ was evaluated using an experimental saturation curve provided by Solvay. S was very close to $7\ 10^{-2}$ for each experiment.

2.3 Sieve analysis

After the steady state was reached, the operation was stopped and the suspension was evacuated from the crystallizer. An image of $NaHCO_3$ crystals, taken using a Scanning Electron Microscope, is presented in Fig.2. The produced crystals were filtered, washed with ethanol and dried. The crystals were then classified in function of their second largest size by sieving in seven size intervals from 0 to 200 µm.

This is the preprint version of a manuscript published in Crystal Research and Technology 45 (2010), no 9, p. 929-938
DOI: 10.1002/crat.201000233
Link: http://onlinelibrary.wiley.com/doi/10.1002/crat.201000233/abstract

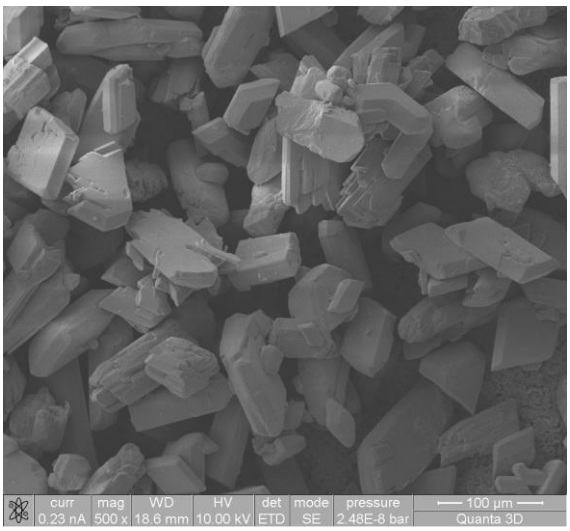

Fig. 2 Photograph of sodium bicarbonate crystals taken using scanning electron microscope.

As presented in Table 1, the i^{th} size interval has a size range from the size L_i to the size L_{i+1}. ΔL_i and $\overline{L_i}$ are the width and the central size of the i^{th} size interval, respectively. They write as follows:

$$\Delta L_i = L_{i+1} - L_i \tag{3}$$

$$\overline{L_i} = \frac{L_i + L_{i+1}}{2} \tag{4}$$

The crystal mass in each size interval was then measured.

Table 1 Description of the size intervals.

Size interval number i	L_i (µm)	L_{i+1} (µm)	ΔL_i (µm)	$\overline{L_i}$ (µm)
1	0	36	36	18
2	36	56	20	46
3	56	63	7	59.5
4	63	90	27	76.5
5	90	112	22	101
6	112	160	48	136
7	160	200	40	180

2.4 Operating conditions

To investigate the influence of solid concentration in suspension on the secondary nucleation rate, specific experimental conditions are required. In laboratory conditions, the reachable solid concentration, by cooling of a saturated solution, is far less than in the industrial conditions (the solid concentration in the industrial column is close to 200 g/kg of suspension). Therefore, a continuous seeding of the crystallizer was realized in order to study the effect of high values of the solid concentration in suspension on the secondary nucleation rate. A well-defined suspension, called the seeding suspension, with a liquid saturated in $NaHCO_3$ at 60°C, was added to the feed solution, at a constant flow rate Q_{seed}, as shown in Fig. 1. Let $n_{seed}(L)$ be the CSD of the crystals in this seeding suspension. It is approximated by:

$$n_{seed}(L) = n_s h(L - L_1) h(L_2 - L) \tag{5}$$

where L is the crystal size and n_s is the number of crystals per unit volume of the seeding suspension in the size interval $[L_1, L_2]$. h is the unit step function [9], L_1 = 63µm and L_2 = 90µm. The values of n_s and Q_{seed} are given

This is the preprint version of a manuscript published in Crystal Research and Technology 45 (2010), no 9, p. 929-938
DOI: 10.1002/crat.201000233
Link: http://onlinelibrary.wiley.com/doi/10.1002/crat.201000233/abstract

in Table 2 for the different solid concentrations in suspension obtained in the crystallizer at steady state. Each experiment was realized twice.

In the study of the relation between the mixing and the secondary nucleation rate in the stirred tank crystallizer, three different mixing conditions were carried out with different rotation speeds and materials. Two propellers were used, with a diameter of 8 cm and 10 cm, respectively. The 10 cm propeller was used at 600 rpm and the 8 cm propeller was used at 600 rpm and 870 rpm. This last rotation speed was chosen in order to induce the same global dissipated power than the 10 cm propeller rotating at 600 rpm. Each experiment was realized once.

The mean residence time τ of the suspension in the crystallizer is the suspension volume in the crystallizer divided by the total flow rate (Q_{feed} for the flow influence study and $Q_{feed} + Q_{seed}$ for the solid concentration influence study).

The experimental conditions are summarized in Table 2.

Table 2 Description of the experiments.

Type of study	Seeding		Propeller diameter (cm)	Rotation speed (rpm)	τ (min)
	Q_{seed} (dm^3/h)	n_s ($m^{-1}m^{-3}$)			
Solid concentration	6	$3.32\ 10^{12}$	8	600	16
	5	$6.26\ 10^{12}$			17
	5	$1.1\ 10^{13}$			17
Flow	No		8	600	26
			8	870	
			10	600	

3 Theoretical developments

3.1 Population balance equation

Mathematical modelling of the CSD in the crystallizer is achieved using Population Balance Equation (PBE), as developed by Randolph and Larson [10].

Let $n(L)$ be the CSD. $n(L)dL$ is the number of crystals in the size interval $[L, L+dL]$ per unit of suspension volume. Let B and G be the secondary nucleation rate and the growth rate of the $NaHCO_3$ crystals, respectively.

It is assumed that the crystallizer is a perfectly mixed constant volume system. The crystal growth rate G is supposed to be independent of the crystal size ($dG/dL=0$). It is assumed that the steady-state is reached and there is no crystal breaking or agglomeration. Preliminary studies have shown that the CSD evolution with the propeller rotation speed from 600 to 870 rpm is characterized only by the crystal growth and nucleation [8].

Whether there is a seeding in the crystallizer feed stream or not, depending on the type of experiment, $n(L)$ is obtained from two different PBE.

When the crystallizer feed stream is free of crystals, the steady state CSD is given by the solution of [1,10,11]:

$$\frac{dn(L)}{dL} = -\frac{n(L)}{G\tau} \tag{6}$$

The analytical solution of Eq. (6), with the condition $n(0) = B/G$ [10], is:

$$n(L) = \frac{B}{G}\exp\left(-\frac{L}{G\tau}\right) \tag{7}$$

When the crystallizer feed stream contains crystals, the steady state CSD is given by the solution of:

$$\frac{dn(L)}{dL} = \frac{1}{G}\left(-\frac{n(L)}{\tau} + \frac{Q_{seed}}{V}n_{seed}(L)\right) \tag{8}$$

This is the preprint version of a manuscript published in Crystal Research and Technology 45 (2010), no 9, p. 929-938
DOI: 10.1002/crat.201000233
Link: http://onlinelibrary.wiley.com/doi/10.1002/crat.201000233/abstract

where V is the suspension volume in the crystallizer and nseed is the seeding CSD (Eq. (5)). The analytical solution of Eq. (8), with $n(0) = B/G$, is:

$$n(L) = \frac{B}{G}\exp\left(-\frac{L}{G\tau}\right) + n_s \frac{Q_{seed}}{V}\tau\left(\left(\exp\left(\frac{L_1 - L}{G\tau}\right) - 1\right)h(L - L_1) - \left(\exp\left(\frac{L_2 - L}{G\tau}\right) - 1\right)h(L - L_2)\right) \quad (9)$$

3.2 Secondary nucleation rate expression

Several semi-empirical correlations can be found in the literature for the contact secondary nucleation rate in a stirred tank. Most of authors showed that the contact secondary nucleation rate is proportional to a power of the volumetric hold-up of the crystals [12-14]. Moreover, when a stirrer rotates in a suspension, the nucleation is proportional to a power of the power provided by the stirrer to the suspension as well [6,15].

Therefore, the following expression is proposed to correlate the secondary nucleation rate B of $NaHCO_3$ crystals to the operational parameters in the stirred tank crystallizer:

$$B = k_b f(T) S^b M_c^m A^q \quad (10)$$

where B is expressed per unit volume of the suspension and per second. M_c is the solid concentration in suspension (mass of crystals divided by the mass of suspension). M_c corresponds to the product of the volumetric hold-up of crystals by the ratio of the suspension density (which is almost constant) on the crystal density. T is the absolute temperature, $f(T)$ is a function of the temperature and A is a (potentially local) property of the flow driving the secondary nucleation rate, such as the dissipated power or the turbulent kinetic energy. The parameters of this model are k_b, m, b and q, which are the nucleation rate constant, the solid concentration exponent, the supersaturation exponent and the flow parameter exponent, respectively.

The objective of this paper is to identify a relevant flow parameter A of this expression and to estimate the value of the m exponent. A value is also estimated for the q exponent. Their values are then qualitatively discussed.

3.3 Modelling of the flow in the crystallizer

The nature of a flow parameter A has to be identified but the local flow properties are generally difficult to measure experimentally. Therefore, they are estimated by the resolution of the Navier-Stokes and continuity equations, supplemented by a turbulence model, using CFD, in order to characterize globally and locally the flow in the stirred tank. The model used for the turbulence modelling is the unsteady k-ε realizable model [16, 17].

The 3-D geometry and the mesh of the crystallizer are generated using the GAMBIT 2.3.16 software. A tetrahedral mesh is used. It is generated using the Tet/Hybrid scheme and the mesh type TGrid is selected. The fluid is separated in two zones: a first zone, called the rotor, delimiting a volume in the vicinity of the propeller inside the draft tube, and a second zone, called the stator, corresponding to the rest of the fluid volume. The mean size of the mesh cells in the stator zone is 4 mm. By the presence of the draft tube, the flow gradients are the largest in the rotor zone. Therefore, the mesh is denser in this zone: the mean size of the cells is 2 mm.

The geometry and the mesh are exported to the FLUENT 6.3.26 software, where the numerical resolution of the equations governing the flow in the tank is performed. The simulations are realized using the sliding mesh method. In the rotor zone, the equations governing the flow are expressed in a rotating reference frame fixed to the mesh. This reference frame rotates around the propeller axis with the same rotation speed (the propeller stays still in this reference frame). In the stator zone, the equations are expressed in a stationary reference frame fixed to the mesh. An interface between the rotor zone and the stator zone has to be defined in the FLUENT software in order to connect the moving mesh of the rotor zone with the stationary mesh of the stator zone.

The settings of the discretization shemes and the solver and solution control parameters are the default settings proposed by the software. The selected time step is the time necessary to make a rotation of 2° around the propeller axis.

This is the preprint version of a manuscript published in Crystal Research and Technology 45 (2010), no 9, p. 929-938
DOI: 10.1002/crat.201000233
Link: http://onlinelibrary.wiley.com/doi/10.1002/crat.201000233/abstract

The simulation results analysis is performed when the simulated flow reaches the steady-state, after 10 rotations of the propeller. The computing time is about 10 days on a single core Xeon processor (2.6 GHz).

3.4 Extraction of kinetics parameters from mass measurements on sieves

The measurement of the crystal mass in the different size intervals allows determining the growth rate *G* and the nucleation rate *B*.

Let $M_{\text{exp}}^{(i)}$ be the mass, determined experimentally, of the crystals having a size in the i^{th} size interval (described in Table 1), per unit volume of the suspension in the crystallizer. This i^{th} interval ranges from L_i to L_{i+1}. If L_i is sufficiently close to L_{i+1}, $M_{\text{exp}}^{(i)}$ can be approached by:

$$M_{\text{exp}}^{(i)} \approx \alpha \rho_S n\left(\overline{L_i}\right) \overline{L_i}^3 \Delta L_i \tag{11}$$

where ρ_S is the crystal density and α is the volume shape factor of the $NaHCO_3$ crystals. α is defined such that αL^3 is the volume of a crystal that has a second largest size equals to *L*. It is determined experimentally by weighing a known number of particles from a narrow size interval [13]. It is observed that α is almost a constant. The value α= 0.3 is obtained.

The classical approach to extract *B* and *G* from the experimental mass measurements consists in estimating the $n(\overline{L_i})$ from the set $M_{\text{exp}}^{(i)}$ using Eq. (11). Plotting the logarithm of the experimentally determined CSD $n(\overline{L_i})$ versus the mean size of the size intervals $\overline{L_i}$, the growth rate *G* is straightforwardly calculated from the slope of the linear trend line and the nucleation rate *B* from the intercept at $L = 0$ of this trend line [11].

Nevertheless, this approach can introduce errors due to the data transformation and is limited to the cases when the feed stream is free of crystals. Therefore, a mass distribution fitting method is used in this work. Rather than to transform the crystals mass measurements into a CSD for comparing to a model, this method consists in using the PBE model to simulate the quantity that is experimentally measured (the mass distribution of the sieve analysis) as a function of *B* and *G*.

Therefore, this method allows estimating *B* and *G* values by comparing the simulated mass distribution with the experimental results. Moreover, this approach is usable with or without crystals in the crystallizer feed stream.

For given experimental conditions reported in Table 2, if values are given to *B* and *G*, the solution of Eq. (6) or Eq. (8) can be used to calculate the corresponding theoretical mass of crystals having a size in the i^{th} size interval, per unit volume of the suspension in the crystallizer, written $M_{\text{th}}^{(i)}(B,G)$:

$$M_{\text{th}}^{(i)}(B,G) = \alpha \rho_S \int_{L_i}^{L_{i+1}} n(L,B,G) L^3 dL \tag{12}$$

When the crystallizer feed stream is free of crystals, Eq. (7) allows simplifying Eq. (14) as follows:

$$M_{\text{th}}^{(i)}(B,G) = \alpha \rho_S BG \begin{pmatrix} \exp\left(-\dfrac{L_i}{G\tau}\right)\left(L_i^3 + 3GL_i^2\tau + 6G^2 L_i \tau^2 + 6G^3\tau^3\right) \\ -\exp\left(-\dfrac{L_{i+1}}{G\tau}\right)\left(L_{i+1}^3 + 3GL_{i+1}^2\tau + 6G^2 L_{i+1}\tau^2 + 6G^3\tau^3\right) \end{pmatrix} \tag{13}$$

With crystals in the crystallizer feed stream, Eq. (9) can be introduced in Eq. (12) and the integral in the resulting equation can also be evaluated symbolically. However, the use of this analytically integrated expression for $M_{\text{th}}^{(i)}(B,G)$ can lead to further numerical instability in the proposed procedure. Therefore, $M_{\text{th}}^{(i)}(B,G)$ is computed numerically when crystals are present in the crystallizer feed stream.

The mind of the proposed method is to estimate the *B* and *G* minimizing the difference between $M_{\text{th}}^{(i)}(B,G)$ and $M_{\text{exp}}^{(i)}$, for $1 < i < 7$. They are called B_{fit} and G_{fit}. To achieve this minimization, a cost function [18] is defined as the sum of the squares of the differences between measured mass and theoretical mass in each size interval and it is expressed as follows:

This is the preprint version of a manuscript published in Crystal Research and Technology 45 (2010), no 9, p. 929-938
DOI: 10.1002/crat.201000233
Link: http://onlinelibrary.wiley.com/doi/10.1002/crat.201000233/abstract

$$C_F\left(B,G\right)=\sum_i\left(M_{\text{exp}}^{(i)}-M_{\text{th}}^{(i)}\left(B,G\right)\right)^2 \tag{14}$$

B_{fit} and G_{fit} are calculated by the MATLAB 6.5 routine *lsqnonlin*, which minimizes the cost function by an iterative process. Starting from an initial guess of B and G, the CSD $n(L)$ is calculated. Using this $n(L)$, the theoretical crystal mass in each size interval is calculated. The cost function is then estimated, comparing the measured and the theoretical crystal mass. The routine changes the current values of B and G to compute the cost function again and compares it with the cost function of the previous step. The routine adjusts step-by-step the value of B and G until it finds its global minimum of the cost function.

4 Results and discussion

4.1 Mass distribution fitting

A comparison between the experimental crystal mass distribution and the simulated mass distributions, computed with the B_{fit} and G_{fit} values identified by the mass distribution fitting method, are presented in Fig. 3.

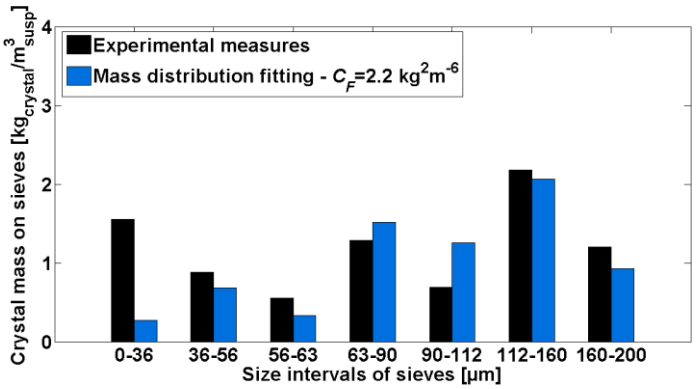

Fig. 3 Comparison of the mass distribution fitting method in terms of mass in size intervals for the case with the 8 cm propeller rotating at 600 rpm without seeding.

In order to check the validity of the solution found by lsqnonlin, an array of value of B and G is generated and the cost function is computed for each pair of B and G values. A cost value surface is then generated. The optimum solution is the lowest point of the surface. The contours of such a surface are presented in Fig. 4. The green point corresponds to the pair of B and G values identified with the mass distribution method and the red one corresponds to those identified with the classical linear regression method. It is observed that the global minimum value of the cost surface is the same than the value found with the *lsqnonlin* routine.

It is important to notice that the mass distribution fitting method is more sensitive to the modelling than the classical approach. It can be observed in Fig. 3 that the mass distribution fitting method does not fit the mass measurements well for the first and the third size interval. The PBE model is likely not sophisticated enough, especially concerning the growth rate G but it does not invalidate the mass distribution fitting method for the B value identification. This point will be further investigated in a future work devoted to the growth rate study.

This is the preprint version of a manuscript published in Crystal Research and Technology 45 (2010), no 9, p. 929-938
DOI: 10.1002/crat.201000233
Link: http://onlinelibrary.wiley.com/doi/10.1002/crat.201000233/abstract

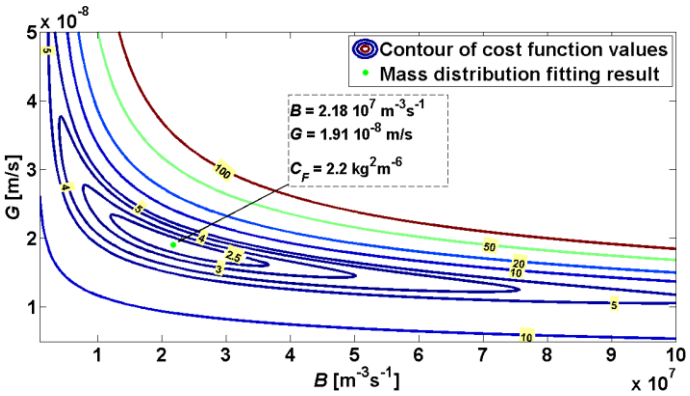

Fig. 4 Contours of the cost function values for a set of B and G values when the 8 cm propeller rotating at 600 rpm is used and without seeding.

4.2 Influence of the solid concentration in suspension on the secondary nucleation rate

Several studies have shown that an increase of the solid concentration in suspension can promote the secondary nucleation rate [19-23] by increasing the number of stable nuclei.

The values of B identified by the mass distribution fitting method are used in this section. $\log(B)$ is plotted against $\log(M_c)$. Using the following equation, the exponent m is estimated by measuring the slope of the linear trend line:

$$\log(B) = m\log(M_c) + \log(k_b f(T) S^b A^q) \tag{15}$$

This analysis is presented in Fig. 5. The exponent m=1.4 is estimated. According to the literature, a value of m close to 1 suggests that the main source of secondary nucleation is due to a crystal-propeller contact mechanism whereas a value close to 2 indicates a crystal-crystal contact mechanism [6,13]. The value m=1.4 suggests that the mechanism of the secondary nucleation is intermediate between crystal-crystal and crystal-propeller shock processes.

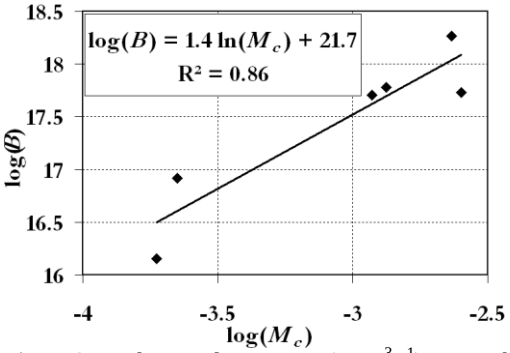

Fig. 5 Secondary nucleation rate (in $m^{-3}s^{-1}$) versus the solid concentration in suspension (in kg/m^3).

4.3 Influence of the flow on the secondary nucleation rate

It is well known that the crystallization kinetics depends on the flow in the reactor [6,20,22,24]. However, the flow parameter that drives the secondary nucleation rate is usually difficult to define. In some cases, it is enough to correlate the nucleation rate with the global power provided by the propeller to the suspension, calculated classically by the following expression [19,24,25]:

$$P = N_p \rho N^3 d^5 \tag{16}$$

This is the preprint version of a manuscript published in Crystal Research and Technology 45 (2010), no 9, p. 929-938
DOI: 10.1002/crat.201000233
Link: http://onlinelibrary.wiley.com/doi/10.1002/crat.201000233/abstract

where N_p is the power number of the propeller, ρ is the suspension density, N is the rotation speed and d is the impeller diameter. A generic value of the power number for the 3-pale marine propellers is N_p=0.35 [6]. This value can only be considered as being a good order of magnitude, as it does not take into account the presence of the draft tube.

The global powers calculated with Eq. (16) are first compared to the estimations from the CFD simulations. A reasonable agreement is observed in Table 3, the differences between the two methods are not larger than 30%.

Table 3 Global dissipated power and estimated nucleation rates for each case in the flow influence study.

Experimental conditions	Global dissipated power (W/m^3)		B ($m^{-3}s^{-1}$)	ε_{edge} (m^2s^{-3})
	Eq. (18)	CFD		
8 cm propeller 600 rpm	315	459	$9.3\ 10^6$	9
8 cm propeller 870 rpm	962	1397	$1.3\ 10^7$	29
10 cm propeller 600 rpm	962	1235	$2.2\ 10^7$	118

The solid concentration M_c of each experiment is close to 0.019. It is clearly observed that the average nucleation rate is not correlated with the global dissipated power, estimated by Eq. (16) or by CFD.

Several local flow parameters, such as the local dissipated power, the flow rate induced by the propeller or the liquid velocity on the propeller blades, at different positions on the propeller, are estimated from the CFD simulations of the stirred tank crystallizer and are compared with the measured nucleation rates B.

It is found that a parameter which is correlated with the nucleation rate measurements is the turbulent kinetic energy dissipation rate ε at the edge of the propeller blade, as shown in Fig. 6. It is noted ε_{edge}. The values of ε_{edge}, for each experiment, are as well presented in Table 3. The contours of the turbulent dissipation rate on the propeller surface are presented in Fig. 7.

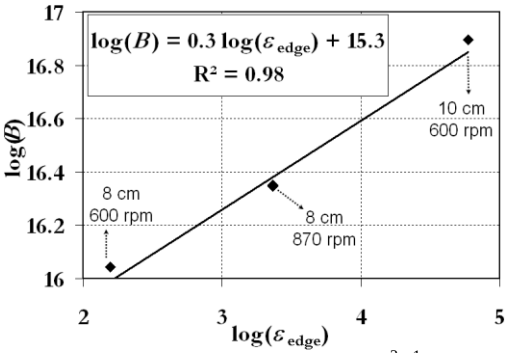

Fig. 6 Secondary nucleation rate (in $m^{-3}s^{-1}$) versus the local turbulent kinetic energy dissipation rate (in m^2s^{-3}) on the edge of the propeller computed from CFD simulations.

As described in the previous section, the mechanism of the secondary nucleation seems to be intermediate between crystal-crystal and crystal-propeller shock processes.

The edge of the propeller is the nearest zone from the inside of the draft tube, on which the suspension is blasted. The power dissipation is maximal in this zone. It creates the smallest Kolmogorov eddies in the suspension and induces the highest crystal-crystal collision frequency [3]. Therefore, from this crystal-crystal shock mechanism, added to the crystal-propeller and the crystal-draft tube collision processes, the propeller edge zone becomes the main source of secondary nucleation.

This is the preprint version of a manuscript published in Crystal Research and Technology 45 (2010), no 9, p. 929-938
DOI: 10.1002/crat.201000233
Link: http://onlinelibrary.wiley.com/doi/10.1002/crat.201000233/abstract

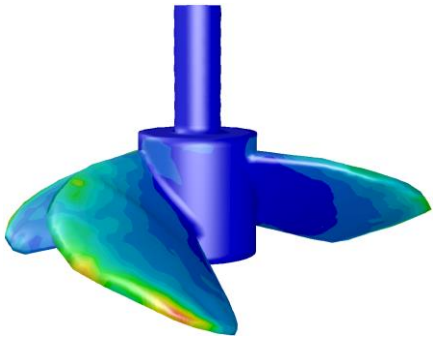

Fig. 7 Contours of the turbulent kinetic energy dissipation rate on the propeller surface (deep blue: 3 m^2/s^3 – red: 118m^2/s^3) computed by the FLUENT simulation for the 10 cm diameter propeller rotating at 600rpm.

A first attempt to quantify the influence of the turbulent dissipation rate in the propeller edge zone on the secondary nucleation rate is realized, plotting log(B) against log(ε_{edge}) in Fig. 6. Using the following equation, the exponent q is calculated by measuring the slope of the linear trend line:

$$\log(B) = q\log(\varepsilon_{edge}) + \log(k_b f(T) S^b M_c^m) \quad (17)$$

The estimated value of the exponent is q=0.3. This value does not quantitatively correlates the secondary nucleation rate and the turbulent dissipation rate since a full investigation of this dependence requires more experiments. Nevertheless, the obtained value can be qualitatively discussed.

The characteristics of the smallest eddies (inverse of size, time of contraction,…) are proportional to a power of the turbulent kinetic energy dissipation rate ε and the typical values of the ε exponent are between 0.25 and 0.5 [16,26]. Therefore, the value found for q suggests that the mechanism of the secondary nucleation rate is, at least partially, related to crystal-crystal shocks in the smallest eddies near the edge of the propeller.

5 Conclusion

The combination of the experimental measurements in the stirred tank crystallizer, the extraction of the kinetic parameters using a mass distribution fitting method and the numerical estimations of local flow properties from CFD simulations allows getting a qualification and a partial quantification of the influences of the solid concentration in suspension and showing a relation between a local mixing parameter and the secondary nucleation rate of the sodium bicarbonate. The undetermined flow parameter of the proposed nucleation rate kinetic expression is identified. The exponent of this parameter and the exponent of the solid concentration in the suspension in this expression (see Eq. (10)) are estimated.

A mass distribution fitting method is used to extract the crystallization kinetics from the experimental mass measurements since it is more general than the classical linear regression method. It can be used to identify the kinetic parameters of different type of PBE and should lead to more accurate results as no conversion of the experimental data is required. All the B estimations, which are used to investigate the influence of solid concentration and mixing on the secondary nucleation rate, are extracted using this method.

The exponent of the solid concentration in suspension in the B expression is estimated and its value is m=1.4. This suggests an intermediate mechanism between crystal-crystal and crystal-propeller collisions.

Concerning the flow influence on B, the combination of the estimation of B from experimental results and the CFD simulation estimations leads to the identification of a flow parameter correlated with B in the stirred tank crystallizer. In the proposed model (Eq. (10)), A is identified as the turbulent kinetic energy dissipation rate on the edge of the propeller blade ε_{edge}. The turbulent dissipation rate exponent in the B expression is calculated and its value is q=0.3 that suggests a mechanism related, at least partially, to crystal-crystal shocks close to the edge of the propeller. Therefore, it is showed that the secondary nucleation rate is related to a local mixing parameter and more experiments has to be performed using the procedure presented in this paper for a full investigation of the mixing influence.

The influence of the temperature and the supersaturation on B and G and will be studied in a future work and a model for G will be proposed.

This is the preprint version of a manuscript published in Crystal Research and Technology 45 (2010), no 9, p. 929-938
DOI: 10.1002/crat.201000233
Link: http://onlinelibrary.wiley.com/doi/10.1002/crat.201000233/abstract

The results of this work will be useful to understand the behaviour of an industrial bubble column reactor, where the energy dissipation is similar (between 600 and 1000 W/m^3) but the local flow properties are likely different and the solid concentration in suspension reaches higher values (about 200 g per kg of suspension). The overall study will be realized stepwise. In a first step, the secondary nucleation rate measurement in the stirred stank crystallizer will be compared to measurements performed using a laboratory scale bubble column recently developed. As it is showed in this work, the relevant mixing parameter can be a local parameter. Therefore, the experiments will be coupled with CFD simulation analysis.

Acknowledgements Authors acknowledge Solvay S.A. for the financial and scientific support, as well as the technical facilities provided by M. Guy Mannaert (Aero-Thermo-Mechanics Department of ULB). Research fellow Christophe Wylock acknowledges financial support from the F.R.S.-FNRS (Belgian National Fund for Scientific Research).

References

[1] Y. Zhu, Etude expérimentale de la cristallisation du bicarbonate de soude, Phd Thesis (Université Libre de Bruxelles, 2004).
[2] B. Haut, Contribution à la modélisation des colonnes à bulles mettant en oeuvre une réaction de précipitation, Phd Thesis (Université Libre de Bruxelles, 2003).
[3] A. t. Cate, J. J. Derksen, H. J. M. Kramer, G. M. v. Rosmalen and H. E. A. V. d. Akker, Chem. Eng. Sci. **56**, 2495 (2001).
[4] P. A. Barata and M. L. Serrano, J. Cryst. Growth **163**, 426 (1996).
[5] E. Kougoulos, A. G. Jones and M. Wood-Kaczmar, Chem. Eng. Res. & Des. **83**, 30 (2005).
[6] A. Mersmann, Crystallization technology handbook, 2nd edition (Marcel Dekker Inc., New York, 2001).
[7] A. Mersmann, F. Werner, S. Maurer and K. Bartosch, Theoretical prediction of the minimum stirrer speed in mechanically agitated suspensions, Chem. Eng. & Proc. **37**, 503 (1998).
[8] V. Gutierrez, Etude de la cristallisation du bicarbonate de sodium raffiné : contribution au modèle des colonnes à bulles, Phd Thesis (Université Libre de Bruxelles, 2010).
[9] M. Abramowitz and I. A. Stegun, Handbook of Mathematical Functions (Dover Publications, New York, 1972).
[10] A. D. Randolph and M. A. Larson, Theory of particulate processes (Academic Press, New York, 1971).
[11] J. Garside, Chem. Eng. Sci. **40**, 3 (1985).
[12] J. Garside and M.B. Shah, Ind. Eng. Chem. Process Des. Dev. **19**, 509 (1980).
[13] J. W. Mullin, Crystallization, 4th edition (Butterworth Heinemann, Oxford, 2002).
[14] A.S. Myerson and R. Ginde, Handbook of Industrial Crystallization, 2nd edition (Butterworth Heinemann, Oxford, 2002).
[15] A.G. Jones, Crystallization Process Systems (Butterworth Heinemann, Oxford, 2002).
[16] S. B. Pope, Turbulent flows (Cambridge University Press, Cambridge, 2000).
[17] ANSYS, Fluent User's Guide, 2006.
[18] E. Walter and L. Pronzato, Identification of parametric models from experimental data (Springer, Berlin, 1997).
[19] C. Gahn and A. Mersmann, Powder Technology **85**, 71 (1995).
[20] C. Gahn and A. Mersmann, Chem. Eng. Sci. **54**, 1283 (1999).
[21] M. Matsuoka, J. Chem. Eng. Japan **35**, 1025 (2002).
[22] Z. Sha and S. Palosaari, Chem. Eng. Sci. **55**, 1797 (2000).
[23] M. Liiri, T. Koiranen and J. Aittamaa, J. Cryst. Growth **237-239**, 2188 (2002).
[24] J. Franke and A. Mersmann, Chem. Eng. Sci. **50**, 1737 (1995).
[25] J. Pohlisch and A. Mersmann, Chem. Eng. & Tech. **11**, 40 (1988).
[26] G.K. Batchelor, H.K. Moffatt and M.G. Worster, Perspectives in Fluid Dynamics (Cambridge University Press, Cambridge, 2002).

This is the preprint version of a manuscript published in Crystal Research and Technology 45 (2010), no 9, p. 929-938
DOI: 10.1002/crat.201000233
Link: http://onlinelibrary.wiley.com/doi/10.1002/crat.201000233/abstract